applied sciences

MDPI

Article

Numerical Study of Low-Temperature Ventilation Drying in a Wheat Grain Silo Considering Non-Uniform Porosity Distribution

Deqian Zheng [1,2,3], Liang Li [1], Guixiang Chen [1,2,3,*], Yang Zhou [1] and Kuo Liu [1]

[1] College of Civil Engineering, Henan University of Technology, Zhengzhou 450001, China; deqianzheng@haut.edu.cn (D.Z.); 202191021@haut.edu.cn (L.L.); robertzhouy@haut.edu.cn (Y.Z.); liudaxiand@icloud.com (K.L.)
[2] Henan International Joint Laboratory of Modern Green Ecological Storage System, Zhengzhou 450001, China
[3] Henan Key Laboratory of Grain Storage Facility and Safety, Zhengzhou 450001, China
* Correspondence: cgx@haut.edu.cn

Abstract: The temperature and moisture content inside a grain pile are two important indicators for judging the safety of grain storage. To accurately predict the temperature and moisture content inside a grain pile, a numerical simulation was carried out of the drying process of a mesoscale wheat grain soil based on a thin-layer drying method, considering non-uniform porosity. The effectiveness of this method for wheat piles was verified through a comparison with the experimental data. The influence of different ventilation cage heights and ventilation temperatures on heat and moisture transfer in the wheat grain pile were also studied. The results show the following points. The numerical simulation method in this paper can effectively predict the temperature and moisture content of a wheat grain pile. The non-uniform porosity distribution model can better reproduce the state of ventilation during storage of wheat grain piles than the uniform porosity distribution model. The distribution patterns of flow lines in silos with different ventilation cage heights have certain similarities, but the high-speed airflow area will decrease as the height of the ventilation cage increases. Different ventilation temperatures will significantly affect the areas of high temperature and the rewetting inside a wheat grain pile.

Keywords: mesoscale wheat grain pile; thin-layer drying; porosity; numerical simulation; heat and moisture transfer

Citation: Zheng, D.; Li, L.; Chen, G.; Zhou, Y.; Liu, K. Numerical Study of Low-Temperature Ventilation Drying in a Wheat Grain Silo Considering Non-Uniform Porosity Distribution. *Appl. Sci.* **2024**, *14*, 96. https://doi.org/10.3390/app14010096

Academic Editor: Francesca Scargiali

Received: 9 November 2023
Revised: 18 December 2023
Accepted: 20 December 2023
Published: 21 December 2023

1. Introduction

China is a major wheat-growing country, and the annual production output of wheat is over 130 million tons [1]. The safe storage of wheat is crucial for national security. This requirement has become more important with the intensification of the Russia–Ukraine conflict and the current Palestinian–Israeli conflict [2,3]. However, when the moisture content of wheat is above the safe level of 14% during storage, the number of pests and mold will sharply increase. This can result in local mold and heating in the wheat pile, which can contribute to quality degradation [4]. To ensure wheat quality during storage, the wheat pile must be kept below a safe moisture level and at an appropriate temperature [5]. A viable solution to counteract these problems is the application of low-temperature ventilation drying [6]. This approach reduces the temperature and humidity of the air around the grain particles by forming airflow circulation within the grain pile. Then, the air undergoes heat and humidity exchange with the grain particles to achieve the goal of reducing the temperature and moisture content of the grain pile [7]. Therefore, studying the drying behaviors of the low-temperature drying of wheat grain piles is crucial for the safe storage of wheat.

The distribution of porosity inside the grain pile is a key parameter that affects the heat and water transfer inside the grain pile during the process of drying. The airflow circulation inside the grain pile is mainly carried out through the connected pores between

particles [8–10]. As the depth of the grain pile increases, the vertical pressure increases, which makes this phenomenon more obvious [11]. Previous studies have shown that the porosity will gradually decrease as the depth of the grain pile increases, which indicates that the resistance of the airflow passing through this area will increase [12–14], reducing the drying efficiency. Simply treating the porosity of the grain pile as a uniform distribution will lead to inaccurate predictions of the grain pile temperature and moderation during numerical simulation [15]. Moreover, compared with the cooling results of grain with a uniformly distributed porosity inside the pile, it has been demonstrated that the cooling time for grain with a non-uniform porosity increased by 55% [16]. In addition, as the depth of the grain pile increases, the effect of self-compaction also increases, resulting in the air velocity decreasing [17]. Although researchers have provided many contributions in terms of the distribution of non-uniform porosity, most scholars have focused on the influence of porosity on the distribution of airflow velocity and airflow resistance; the effect on the heat and moisture transfer inside the grain pile is rarely reported.

Considering the influence of non-uniform porosity in the simulation of the low-temperature drying of a wheat grain pile is not enough for prediction accuracy, and the selection of the drying model is more important. However, the heat and moisture transfer inside the grain pile during the drying process is complex [18]. For this reason, many drying models have been used to study the drying process for wheat grain piles [19]. There are more than 100 different thin-layer drying models based on semi-theoretical models and the empirical models used in grain piles under different drying conditions [20]. For the semi-theoretical models, researchers have usually proposed the drying models based on Newton's law of cooling, Fick's second law of diffusion [21–26], and relevant experiments. For the empirical models, scholars have derived models from relevant experimental data, such as the Wang and Singh model, the Thompson model, the Weibull distribution models, etc. [27–29]. Compared with the empirical models, the semi-theoretical models consider the fundamentals of the drying process, so they do not require assumptions regarding the geometry of a typical grain and are more suitable for the drying of porous media [30]. Moreover, the semi-theoretical models have fewer limitations in simulating the drying process of wheat piles compared with the empirical model, as they consider the related theories [30].

Previous studies have indicated that the distribution of porosity and the drying model have a significant impact on the heat and moisture transfer inside a wheat pile. However, the literature is still lacking in terms of the process of drying inside a mesoscale wheat pile based on the thin-layer drying models, especially under the condition of non-uniform porosity. Therefore, this study took a wheat grain pile of a mesoscale silo as the research object. The drying behaviors inside the wheat grain pile of a mesoscale silo were studied through a self-designed program leading into the thin-layer drying model based on the heat and mass transfer theory of porous media. The effect of different porosities on the drying process was also studied. The effectiveness of this numerical simulation method was verified by comparing the numerical simulation results with the experimental result. In addition, the effect of different ventilation cage heights, ventilation temperatures, and ventilation rates on the temperature and moisture changes in wheat grain piles were also studied.

2. Materials and Methods

2.1. Materials

The wheat used in this study was Zhoumai 22 hybrid wheat, harvested in 2021. The harvested wheat was filtered through a pneumatic conveyor to remove the broken kernels and foreign impurities. The average moisture content was approximately 12.5%, and the average density of wheat in the silo was approximately 800 kg/m^3.

2.2. Experimental Apparatus

The heat and moisture transfer test of the wheat grain pile in the silo adopts the multi-field coupling simulation test platform built by the research group. The platform is

composed of six parts: the grain storage silo, ventilation regulation system, servo flexible loading control system, constant temperature control system, temperature detection system, and computer control system. There is a cavity region at the bottom of the silo, and ventilation cages near the silo walls were connected to that area. Small circular holes with a diameter of 3 mm were evenly distributed on the surface of the ventilation cage. The air flow was pressed by the fan and filled the cavity region at the bottom of the silo. Then, the air flow entered the ventilation cage near the wall of the silo and continued to move upwards along the height of the ventilation cage, entering the interior of the grain pile from the holes on the surface of the ventilation cage. Finally, the air flow was discharged through the air outlet on the top of the silo (as shown in Figure 1c).

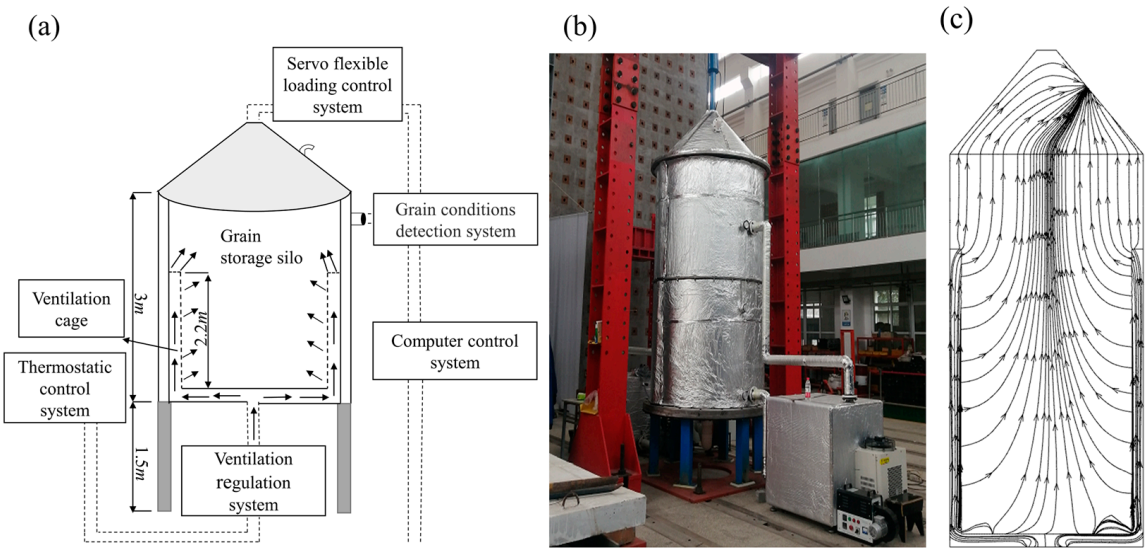

Figure 1. Schematic diagram of the composition of the multi-field coupling test platform for the grain storage environment: (**a**) platform system; (**b**) grain storage cylinder; (**c**) ventilation path.

As is shown in Figure 1b, the grain storage silo consists of a cylindrical body and a conical roof. The inner diameter of the silo is 1.5 m, the height is 3.0 m, and the maximum grain loading height is 3.0 m. Four sensor cable outlets and five sampling ports were installed on the wall of the soil. The height of the warehouse top was 0.8 m, with a slope of 45°. Two vents and servo flexible loading control system loading ports were reserved. The insulation materials were used on the outer surface of the experimental silo to ensure the heat insulation performance. Four air ducts with a height of 2.2 m and an aperture of 3 mm at equal intervals were set into the inner wall of the silo. To eliminate errors caused by the sensor's movement during grain loading, a horizontal bracket was installed on each layer inside the silo to fix the position of the temperature sensor.

The drying method used in this paper was low-temperature ventilation drying. The temperature control system regulated the temperature and humidity of the ambient air sucked in by the axial flow fan. After reaching the set target temperature and stabilizing it, the ventilation system was activated to send cold air into the interior of the grain pile through a ventilation cage at the inner wall of the silo, and the cold air supplied to the wheat piles exchanged the heat with the grain particles to achieve the cooling effect in the grain pile. To ensure that the temperature of the ventilation air was lower than that of the wheat pile, a refrigeration machine was used to control the ventilation temperature. To reduce the impact of the environmental temperature on the supply air temperature and humidity inside of external pipelines during the ventilation process, insulation treatment was carried out on it. The outer walls of the silo and its bottom were also thermally insulated to reduce the impact of the environmental temperature.

To study the variation in temperature and water content inside the wheat grain pile under ventilation, each system of the test platform was inspected and debugged using

measuring instruments before testing. The temperature sensors were arranged according to the test plan. A total of fourteen temperature sensors are arranged inside the silo to record temperature changes at different positions. One temperature and one humidity sensor in the air inlet at the bottom of the silo were installed to record the temperature and humidity of the diffuser, respectively. The sensors position was shown by the red dot in Figure 2. Of note, the measured data were also used as the inlet boundary conditions for numerical simulation research in a later section. The measurement point positions are shown in Figure 2.

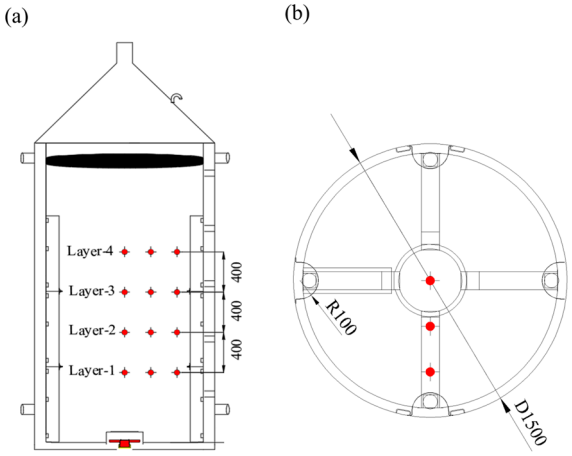

Figure 2. Schematic diagram of measurement points: (**a**) vertical section measurement point position; (**b**) horizontal section measurement point position.

2.3. Numerical Simulation Models and Methods

2.3.1. Fluid Transport Equations

Generally, the grain piles were considered as porous media when conducting numerical simulation research on mechanical ventilation [31]. The control equations for internal flow and coupled heat and moisture transfer in grain piles will now be given.

The continuity equation is obtained as follows [32]:

$$\frac{\partial(\varepsilon\rho_a)}{\partial t} + \nabla \cdot (\varepsilon\rho_a \vec{v}) = 0 \tag{1}$$

where ε is the porosity; ρ_a is the air density; t is the time; $\vec{v}$ is the vector velocity of air; and ∇ is a vector symbol representing divergence.

The moisture transfer equation is expressed as [33]:

$$\frac{\partial(\varepsilon\rho_a w)}{\partial t} + \nabla \cdot (\varepsilon\rho_a \vec{v} w) = \nabla \cdot (\varepsilon\rho_a D_{eff} \nabla w) + S_w \tag{2}$$

where w is the absolute moisture content in the air between grains; D_{eff} is the effective diffusion coefficient of water vapor; and S_w represents the moisture source terms for the moisture absorption and desorption of grain particles in the porous medium domain of grain piles, which can be expressed as:

$$S_w = (1-\varepsilon)\rho_t \frac{\partial W}{\partial t} \tag{3}$$

where W is the moisture in wheat piles, and ρ_t is the density of the grain kernels on a dry basis.

The momentum conservation equation was expressed as [34]:

$$\frac{\partial(\varepsilon\rho_a \vec{v})}{\partial t} + \nabla \cdot (\varepsilon\rho_a \vec{v}\vec{v}) = -\varepsilon\nabla p + \nabla \cdot (\varepsilon\mu\nabla\vec{v}) + S_i \tag{4}$$

where ∇p is the pressure gradient; μ is the air viscosity; and S_i is the source term of the momentum equation in the porous media of grain piles, which can be expressed as:

$$S_i = -(\frac{\mu}{\alpha}\vec{v} + \frac{C_2\rho_a}{2}\left|\vec{v}\right|\vec{v}) \tag{5}$$

where μ is the air viscosity, α is the viscous resistance coefficient, and C_2 is the inertial drag coefficient. The viscous resistance coefficient and the inertial drag coefficient can be expressed as follows:

$$\frac{1}{\alpha} = \frac{150\mu(1-\varepsilon)^2}{dp^2\varepsilon^3}\nu \tag{6}$$

$$C_2 = \frac{150\mu(1-\varepsilon)^2}{dp^2\varepsilon^3}\nu + \frac{1.75\rho_a(1-\varepsilon)}{dp\varepsilon}\nu^2 \tag{7}$$

The energy transfer equation based on the local equilibrium heat model of porous media (air temperature equal to grain temperature) is expressed as [34]:

$$\frac{\partial(\varepsilon\rho_a C_{pa}T_a + (1-\varepsilon)\rho_g C_{pg}T_a)}{\partial t} + \nabla\cdot(\varepsilon\rho_a\vec{v}C_{pa}T_a) = \nabla\cdot(\varepsilon k_{eff}\nabla T_a) + S_h \tag{8}$$

where ρ_g is the volume density of the grain piles; T_a is the temperature; K_{eff} is the effective thermal conductivity of the grain pile; and S_h is the energy source term for the grain pile domain, which can be expressed as:

$$S_h = (1-\varepsilon)\rho_t\frac{\partial W}{\partial t}h_v \tag{9}$$

where h_v is the latent heat of evaporation of water.

2.3.2. Thin-Layer Drying Model

The drying of the grain pile is a complex process that involves both heat and moisture transfer. A modified dual-parameter thin-layer drying model was used in this paper to study the drying behaviors inside the wheat pile during mechanical ventilation. The modified dual-parameter model can be expressed as follows [18]:

$$\frac{\partial W}{\partial t} = -knt^{n-1}(W - We) \tag{10}$$

where t is the time, and its unit is minutes; k and n are the empirical coefficients of the grain drying model, respectively, which can be expressed as $k = 2.8\times10^{-3}\times e^{0.059T}\times r^{-0.139}\times v^{0.025}$ and $n = 0.784$, respectively; We is the equilibrium moisture for the dry basis grain; W is the dry basis moisture of the grain at time t; r is the relative humidity of dry air; $r \le 0.99$, v is the dry air velocity; and T is the temperature of the dry air.

The semi-empirical equation of equilibrium moisture is as follows [18]:

$$We = (C_1 + C_2T)(\frac{r}{1-r})^{\frac{1}{C_3}} \tag{11}$$

where C_1, C_2, and C_3 are the empirical coefficients of the model, with values of 0.129, -6.460×10^{-4}, and 2.944 [18], respectively.

2.3.3. Mesh Model and Parameter Settings

To ensure comparability with the experimental results, the scale of the CFD model and the experimental model is 1:1, as shown in Figure 3. A tetrahedral mesh partitioning scheme was adopted after optimizing the geometric model of the silo. The total grid number was 680,000, and the transient calculation time step (i.e., time interval) was set as 6 s.

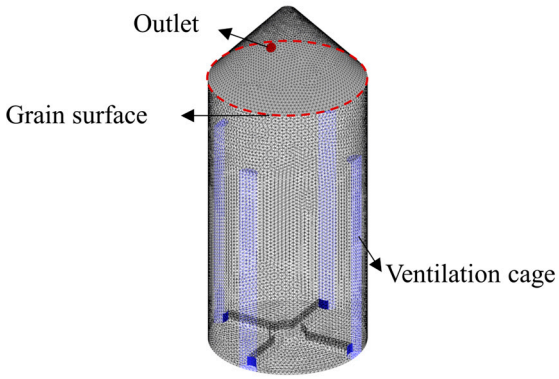

Figure 3. Geometric mesh of the numerical model.

The inlet of the model of numerical simulation was set as the mass flow inlet with the value of 0.51 kg/s. The outlet of the numerical model was set as the pressure outlet. Considering that the walls of the silo were all insulated during the experiment, the wall of the silo for the numerical simulation was set as a non-slip adiabatic wall. To maintain consistency with the experiment, the initial temperature of the wheat pile in the numerical simulation was defined based on the average temperature of each layer measured experimentally before conducting low-temperature ventilation drying. The initial temperature of the first layer was 33.7 °C, the initial second layer was 34 °C, the initial temperature of the third layer was 28.4 °C, and the initial temperature of the fourth layer was 25 °C. The density of wheat was set as 800 kg/m^3, and the initial dry basis moisture content was 12.5%. The temperature of drying air was set as 15.7 °C, and its relative humidity was 60%. In addition, the internal pressure caused by self-weight was relatively large due to the 3 m height of the wheat pile, resulting in a non-uniform distribution of porosity inside the grain pile. Therefore, the porous medium model in simulation adopted a non-uniform porosity distribution to maintain consistency with the experiment, and the effect of the uniform porosity condition on numerical simulation results was specially studied here.

Considering both simulation accuracy and time, the convergence residuals of the continuity equation, momentum equation, and air moisture transfer equation were set as 1.0×10^{-3}, and the value for the energy equation was set as 1.0×10^{-6}. The pressure–velocity decoupling method utilizes the SIMPLEC algorithm. The relaxation factor of energy and UDS was set as 0.8, and the transient equation scheme was set as first-order implicit. Moreover, the viscous resistance coefficient and inertial resistance coefficient were calculated using the Ergun equation [35] with values of 2.21×10^7 m^{-2} and 1.15×10^3 m^{-1}, respectively.

The non-uniform porosity distribution formula of wheat grain piles in silos in this study is as follows [19], with the variation range of non-uniform porosity with a depth of 0.37–0.42 being obtained via Equation (10), and the average value of 0.40 being taken as the uniform porosity:

$$\varepsilon = \varepsilon_0 - (\varepsilon_0 - \varepsilon_{\min}) \cdot (1 + 0.016H_b + 0.002t - 1.013) \quad (12)$$

where H_b is the depth of the grain unit body; ε is the porosity of the grain pile at the corresponding depth H_b; ε_0 is the initial porosity; $\varepsilon_{\min}$ is the minimum porosity inside the grain pile, which can be considered as the porosity of the bottom surface of the grain pile; and t is the storage time of wheat, in the numerical simulation of this paper, $t \leq 720$ h .

Before the ventilation test was conducted, the wheat in the silo was subjected to static treatment to achieve an equilibrium state between the temperature of the wheat pile and the temperature of the air inside the pores. Hence, the initial temperature of the wheat piles and the initial temperature of the air inside the wheat piles were set to be the same. Then, the cold air was supplied to the wheat piles through the ventilation cage, and the cold air

entering the inside of the wheat pile would undergo heat exchange with the grain pile to achieve the purpose of drying.

3. Results and Discussion

3.1. Verification of Numerical Simulation Method

The following was carried out in order to verify the effectiveness of numerical simulation methods and study the influence of porosity distribution on the temperature and moisture content distribution of a wheat grain pile under the thin-layer drying model. First, the simulation results were compared with the experimental results. Figure 4 shows the comparison of the experimental and simulated temperature of each layer and the overall average temperature of the wheat pile after 88 h of mechanical ventilation. Overall, the numerical results at various layers agree with the experimental measurements, while the results show that the non-uniform porosity distribution is improved with the trend in the experiment compared with the uniform porosity distribution.

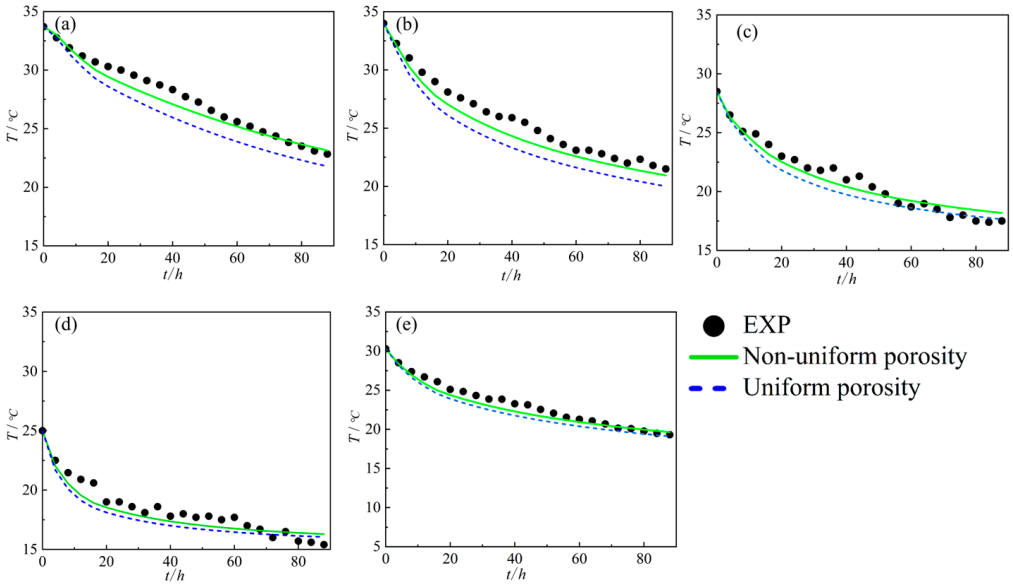

Figure 4. Experiment and simulation comparison of wheat grain pile temperature: (**a**) average temperature of the first layer; (**b**) average temperature of the second layer; (**c**) average temperature of the third layer; (**d**) average temperature of the fourth layer; (**e**) overall average temperature.

The difference in the predicted results between the two porosity distribution models gradually increases as the ventilation time increases, especially at the first layer (Figure 4a). The maximum difference occurs at the moment after the end of ventilation, where the predicted values of the non-uniform porosity distribution model are basically consistent with the experimental results, while the uniform porosity distribution model overestimates a cooling of approximately 1 °C. The reason for the above differences is that the first measurement point is closest to the bottom of the silo, with the smallest porosity under non-uniform porosity distribution (value 0.37), while the corresponding value of the uniform porosity distribution model is 0.40. Therefore, during the ventilation process, the decrease in porosity increases the airflow resistance of ventilation, and the increase in density also increases the heat absorbed by the wheat during drying in this area. Ultimately, the predicted results for the cooling of the non-uniform porosity distribution model during ventilation and cooling are slower compared to the uniform distribution model. For the other layers, as the depth of the grain layer decreases, the difference in porosity distribution between the two models decreases, resulting in the predicted difference between the two porosity distributions also decreasing. The maximum temperature differences from the first layer to the fourth layer were 1 °C, 0.67 °C, 0.45 °C, and 0.27 °C, respectively.

The cooling rate of two porosity distribution models was faster compared with the experimental results. However, the non-uniform porosity distribution model showed better

agreement with the experiment during the entire ventilation process. This was particularly true in the first and second layers of the wheat pile, where the predicted results of the two models differed significantly. For the model with non-uniform porosity distribution, there was a small difference between the simulated and experimental results of each grain layer from 0 h to 10 h and from 60 h to 88 h. The maximum error occurred in the fourth layer with a value of 0.9 °C, while the maximum error value at that area of the uniform porosity distribution was 1.18 °C. During the ventilation period from 10 h to 60 h, there was a relatively large difference between the simulated and experimental results. For the non-uniform porosity distribution, the maximum error occurred in the fourth layer with a value of 1.68 °C, while the corresponding value for the uniform porosity distribution was 1.94 °C. The reason for this is that the experimental conditions were not stable due to environmental factors, the silo structure, and the internal air duct layout. This resulted in significant errors between the experimental and simulated results for each layer at this stage. Additionally, due to the high air velocity in the pores of the wheat particles on the third and fourth layers, the experimental values may first receive the external input of cold air, leading to significant fluctuations.

Although two porosity distribution models can reflect the temperature variation trend in the experimental results, the non-uniform porosity distribution model has a better fit in terms of predicting the temperature change results for the entire ventilation process.

3.2. Influence of Different Ventilation Conditions

Different ventilation conditions will affect the drying behaviors inside the wheat pile under the action of mechanical ventilation. Concerning the low-temperature ventilation drying experiment on the wheat pile mentioned in Section 3.1, the temperature in the middle and lower parts of the wheat pile was higher than that in the other parts. To analyze and solve the problem of an unfavorable temperature distribution during the ventilation process, this section takes the average temperature of 34 °C and water content of 12.5% at the time of wheat storage as the initial conditions. To study the influence of different ventilation cage heights and different ventilation temperatures on the drying behaviors, a typical cross-section of the silo (located at the vertical section of the measurement point arrangement, as shown in Figure 2) was selected to analysis the flow field and temperature field.

3.2.1. Influence of Different Ventilation Cage Heights

This section investigates the effect of different ventilation cage heights on wheat drying, considering a non-uniform porosity distribution. The streamline diagrams of the ventilation cage on the inner wall of the silo at heights of 2.1 m, 1.4 m, and 0.7 m are shown in Figure 5.

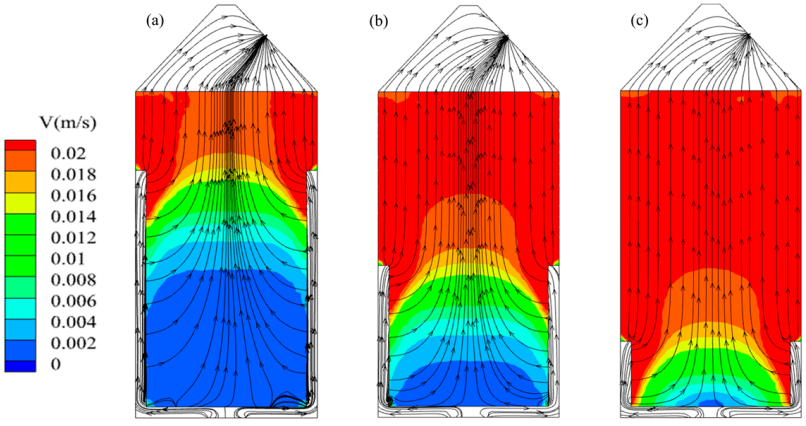

Figure 5. Flow field streamline and velocity distribution: (**a**) 2.1 m; (**b**) 1.4 m; (**c**) 0.7 m.

Overall, the external airflow under three conditions reaches the perforated ventilation cage on the inner wall of the silo along the ventilation duct, and the airflow inside the

cage is divided into two parts. A part of the airflow continues to flow along the height direction of the ventilation cage until it reaches the closed port at the top of the ventilation cage. After entering the interior of the wheat pile along the height direction of the silo, it is discharged from the outlet located at the silo roof. The other part of the airflow enters the interior of the wheat pile, travelling upward radially through the openings on the surface of the ventilation cage. The airflow then converges in the middle of the wheat pile and flows upward along the height direction of the silo, before being discharged from the top outlet of the silo. The difference is that the area affected by radial airflow inside the grain pile becomes larger as the height of the ventilation cage on the inner wall of the warehouse increases. From the perspective of streamline distribution, there is no ventilation dead angle problem in any of the three arrangements. The low-speed distribution area at the bottom of the silo gradually decreases with the decreases in the height of the ventilation. Compared with the other conditions, the airflow distribution inside the wheat pile was relatively uniform when the height of the ventilation cage was 0.7 m.

Figure 6 shows the temperature distribution clouds inside the grain pile at different times when the ventilation cage height on the inner wall of the warehouse was 2.1 m, 1.4 m, and 0.7 m, respectively. The airflow velocity inside the wheat pile below the height of the ventilation cage was relatively small when the height of the ventilation cage was 2.1 m (Figure 6a). The low-temperature airflow entering the grain pile along the surface of the ventilation cage caused the wheat particles on the surface to cool down. Therefore, a phenomenon of a cold skin and a hot core caused by temperature accumulation formed in this region. Although the gathering area of high temperature decreased with the increase in ventilation time, the maximum temperature inside the wheat pile at the end of the ventilation was still as high as 26.9 °C. This indicates the relative inefficiency of the entire 96 h ventilation cooling cycle.

The characteristics of the temperature distribution of the wheat pile when the height of the ventilation cage was 2.1 m were similar when the height of the ventilation cage was 1.4 m (Figure 6b). Although the gathering area of high temperature decreased with the decrease in the height of the ventilation cage, the highest temperature inside the wheat pile also reached 20.6 °C at the end of the ventilation. This indicates that the phenomenon of a cold skin and a hot core still did not disappear. The temperature inside the wheat pile decreased significantly faster than the other two cases when the height of the ventilation cage was 0.7 m (Figure 6c). The highest temperature inside the wheat pile was only 19.4 °C when it was continuously ventilated for 24 h; however, its high-temperature area was located in the middle and upper parts of the wheat layer (the other two cases were located in the middle and lower parts of the two layers). The reason for this is that the lower height of the ventilation cage causes the ventilation in the middle and lower parts of the wheat pile to be more sufficient (as shown in Figure 6). A high-temperature area appears at the end of the air flow in the middle and upper parts of the grain pile, while this phenomenon will gradually disappear as the ventilation time increases.

Overall, different height arrangements of ventilation cages in the inner walls of the silo can cause differences in the temperature distribution inside the wheat pile. According to the analysis above, a ventilation cage height of 0.7 m in the silo had a better cooling effect. Therefore, based on this ventilation arrangement, specific analysis will be conducted on the temperature and moisture content changes in grain piles with different ventilation temperatures in the following section.

3.2.2. Influence of Different Ventilation Temperatures

To study the effect of the ventilation temperature on the distribution of temperature and moisture content inside the wheat pile, numerical simulations were conducted on the wheat pile with an initial temperature of 34 °C and an initial moisture content of 12.50%. Three conditions of different ventilation temperatures of 15 °C, 17 °C, and 19 °C were studied.

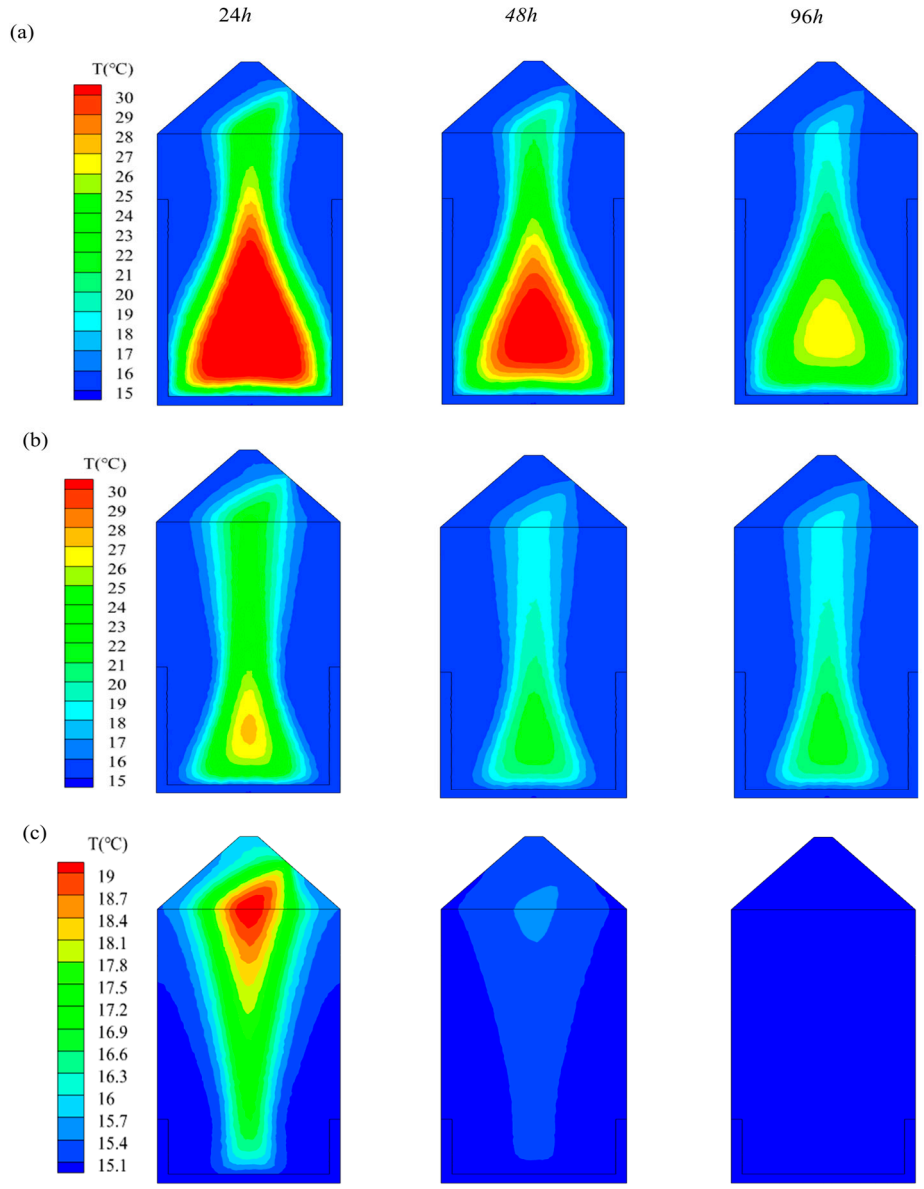

Figure 6. Temperature distribution at different ventilation cage heights: (**a**) 2.1 m; (**b**) 1.4 m; (**c**) 0.7 m.

Figure 7 shows the temperature distribution cloud map inside the wheat pile under continuous ventilation with different ventilation temperatures of 15 °C, 17 °C, and 19 °C for 24 h. The highest temperatures inside the wheat pile of at temperatures of 15 °C, 17 °C, and 19 °C were 29.32 °C, 29.44 °C, and 29.63 °C, respectively. The low-temperature air enters the wheat pile, then generates a strong heat exchange with wheat particles, causing a cold front surface toward the interior of the grain pile. However, the area of the low-temperature cold front inside the wheat pile was smaller due to the shorter ventilation time, and the size of the cold front decreased with the increase in ventilation temperature. The areas of high temperature were all concentrated in the center of the wheat pile, and the area covered by the high temperature increased with the increase in ventilation temperature. This may be due to the fact that the direction of the incoming air flow tends to be horizontal as the height of the ventilation cage decreases, causing low-speed cold air in the middle and lower parts to collect in the middle. Then, they flowed out along the grain surface in an upward direction. When the ventilation temperature increases, the amount of heat absorbed by the cooling airflow decreases, resulting in an increase in the area of high temperature.

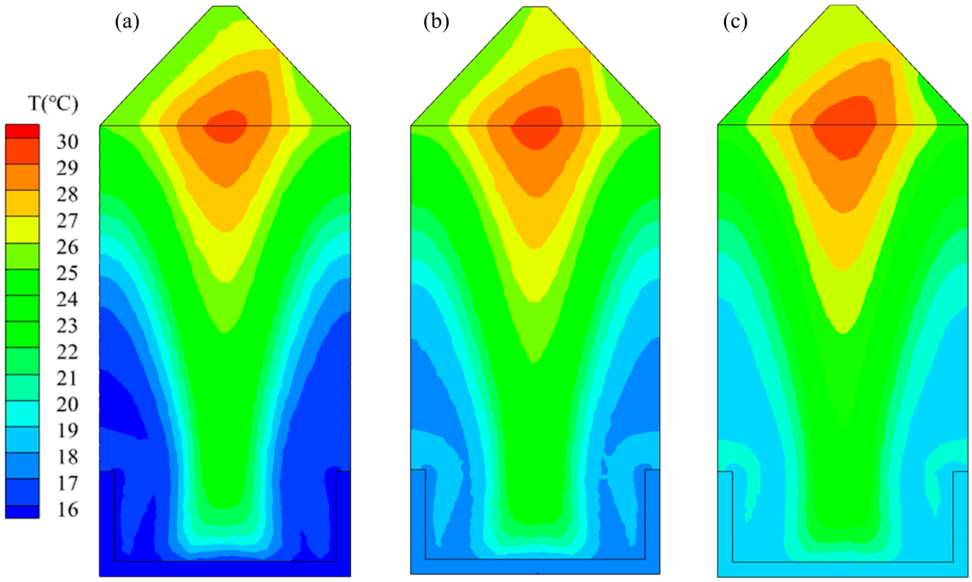

Figure 7. Temperature distribution cloud map for 24 h of ventilation under different ventilation temperatures: (**a**) 15 °C; (**b**) 17 °C; (**c**) 19 °C.

Figure 8 shows the temperature distribution cloud map inside the wheat pile under continuous ventilation with the different ventilation temperatures of 15 °C, 17 °C, and 19 °C for 48 h. At this time, the highest temperature inside the wheat pile at the three temperatures of 15 °C, 17 °C, and 19 °C decreased to 19.97 °C, 20.93 °C, and 21.99 °C, respectively. Compared with the results of the 24 h experiment, the area of the cold front inside the wheat pile gradually increased with the increased ventilation time, and the overall temperature inside the wheat pile significantly decreased. Moreover, the temperature stratification characteristics were also not as obvious as they were at 24 h. In addition, the highest temperature inside the wheat pile represented a ventilation temperature decrease of 15 °C, compared with 9.35 °C at 24 h. This indicates that a lower ventilation temperature causes the temperature inside the wheat pile to decrease faster under the same ventilation rate conditions.

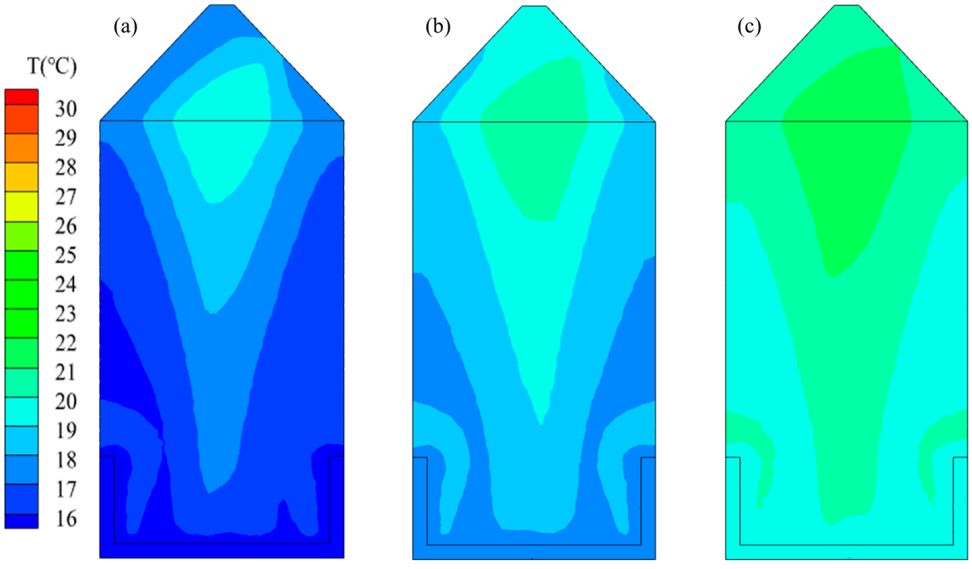

Figure 8. Temperature distribution cloud map for 48 h of ventilation under different ventilation temperatures: (**a**) 15 °C; (**b**) 17 °C; (**c**) 19 °C.

Figure 9 shows the temperature distribution cloud map inside the wheat pile under continuous ventilation with the different ventilation temperatures of 15 °C, 17 °C, and 19 °C for 96 h. With these temperatures of 15 °C, 17 °C, and 19 °C, the highest temperature inside the wheat pile decreased to 16.45 °C, 18.48 °C, and 20.34 °C, respectively. The maximum temperature difference in three cases inside the silo did not exceed 3 °C. The cold front area inside the wheat pile continued to increase as the ventilation time increased. The temperature of most areas inside the wheat pile was consistent, and the area of high-temperature accumulation in the middle of the grain surface also disappeared with the increased ventilation time. However, the high-temperature area near the ventilation cage inside the wheat pile still existed. The reason for this is that the temperature of the wheat pile decreased and the vapor pressure of the air around the grain particles increased when cold air was fed into the grain pile, which promoted moisture absorption and heat release in the wheat particles. Overall, the temperature variation in three cases showed a gradual trend toward a uniform distribution.

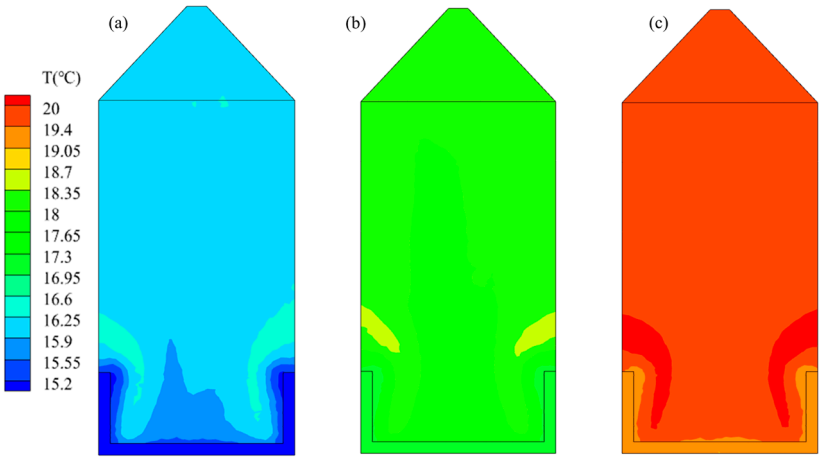

Figure 9. Temperature distribution cloud map for 96 h of ventilation in different ventilation temperatures: (**a**) 15 °C; (**b**) 17 °C; (**c**) 19 °C.

Figure 10 shows the distribution of the dry-basis moisture content in the wheat pile under continuous ventilation conditions at 15 °C, 17 °C, and 19 °C for 24 h. Affected by the cooling cold air, the temperature near the ventilation cage was lower than in the other regions, resulting in a change in the vapor pressure of the air inside the wheat pile. That led the equilibrium moisture content located in this area to be greater than the initial moisture content of the grain. This resulted in the phenomenon of moisture absorption of the wheat particles and the formation of an obvious re-humidification area. The moisture content of the wheat pile in this area increased from the initial 12.50% to 12.80%. Although the relative humidity of ventilation is 60%, the absolute humidity of the supplied air varies due to the different ventilation temperatures, which also affects the water transport inside the grain pile. Moreover, there is a high-temperature-accumulation area in the middle of the grain surface (as shown in Figure 7), and a high degree of moisture also accumulates in this area. The main reason for this is the wheat surface at the end of the ventilation path will exhibit significant hysteresis under the influence of ventilation.

Figure 11 shows the distribution of the dry basis moisture content in the wheat pile under continuous ventilation conditions at 15 °C, 17 °C, and 19 °C for 48 h. Compared with the results at 24 h, the internal moisture content inside the wheat pile was been slightly reduced with the increase in ventilation time. The relatively high moisture content area located in the middle and upper part inside the wheat pile also disappeared. The reason for this is the moisture content inside the wheat pile was low in a ventilation and cooling environment, resulting in a smaller rate of moisture loss. However, the moisture content located near the ventilation cage did not reach the equilibrium moisture content, resulting in the moisture content and its coverage area increasing in this area. Moreover,

the difference in the values of the moisture content between the highest and lowest of the three cases was not very significant inside the wheat pile. But for the distribution of moisture content inside the wheat pile, the area with high moisture coverage in the middle of the grain pile was the smallest when the ventilation temperature was 15 °C.

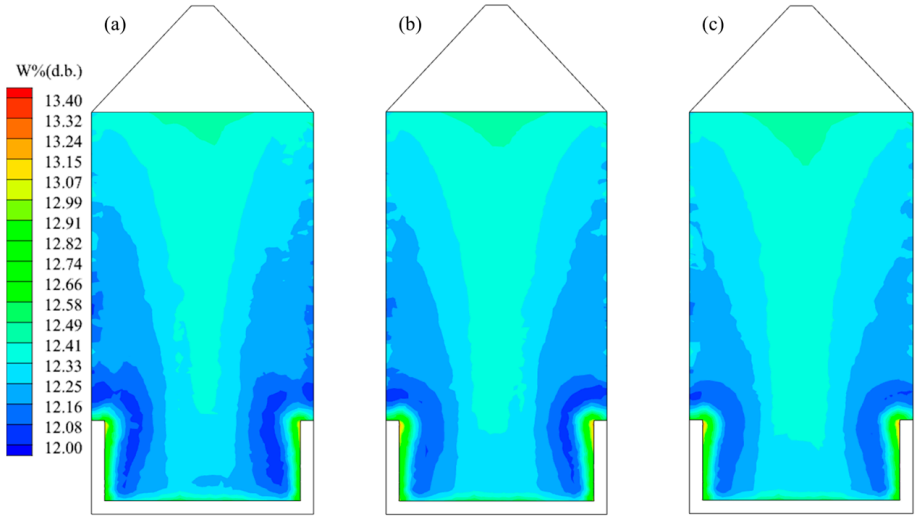

Figure 10. Moisture distribution cloud map for 24 h of ventilation in different ventilation temperatures: (**a**) 15 °C; (**b**) 17 °C; (**c**) 19 °C.

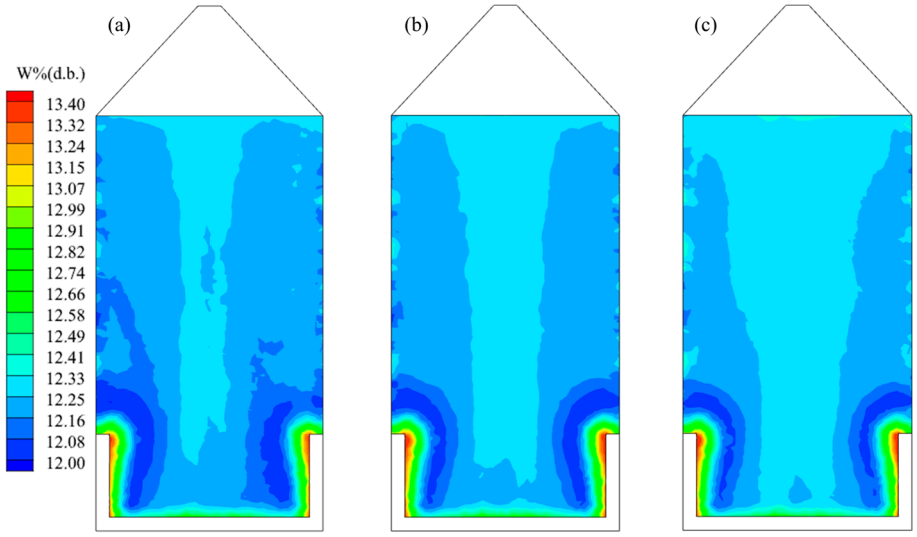

Figure 11. Moisture distribution cloud map for 48 h of ventilation under different ventilation temperatures: (**a**) 15 °C; (**b**) 17 °C; (**c**) 19 °C.

Figure 12 shows the distribution of the dry-basis moisture content in the wheat pile under continuous ventilation conditions at 15 °C, 17 °C, and 19 °C for 96 h. The re-humidification area inside the wheat pile still increased with the increased ventilation time, but the moisture content in the other parts inside the wheat pile gradually stabilized. Moreover, the average moisture content inside the wheat pile under the three temperatures of 15 °C, 17 °C, and 19 °C decreased from the initial 12.50% to 12.28%, 12.29%, and 12.30%, respectively. This indicates that the three ventilation conditions have good water retention effects.

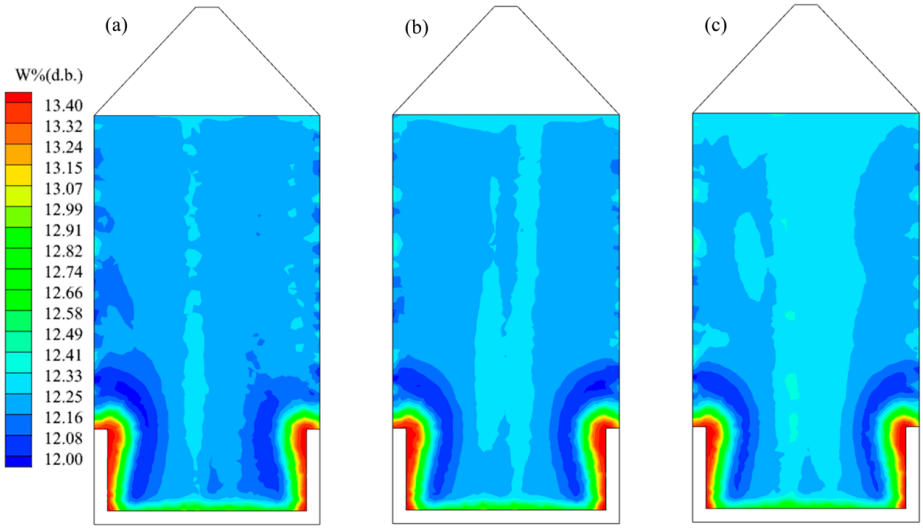

Figure 12. Moisture distribution cloud map for 96 h of ventilation under different ventilation temperatures: (**a**) 15 °C; (**b**) 17 °C; (**c**) 19 °C.

4. Conclusions

We studied the drying behaviors of the low-temperature ventilation and drying of a wheat pile, considering the non-uniform distribution of porosity. A self-designed program based on the thin-layering drying model was carried out to study the influence of non-uniform porosity on the drying process of a wheat pile under different ventilation conditions. The research results can predict and analyze the changes in the temperature field of the wheat piles, facilitating the formulation of effective control measures to reduce grain spoilage during storage, maintain the quality of grain, and ensure the safety of grain storage. The main conclusions drawn are as follows.

1. By comparing the results with experimental data, the present method was verified as being capable of accurately reproducing the temperature and moisture content of a wheat pile inside a mesoscale silo.
2. The non-uniform porosity distribution model can better reflect the actual storage situation inside the wheat grain piles, and its predictive ability in terms of temperature and moisture is also greater than that of the uniform porosity distribution model.
3. For different ventilation cage heights, there is a certain similarity in the distribution of flow lines in silos. Some of the airflow will directly enter the wheat pile after entering the ventilation cage, while the other parts will flow along the height direction of the ventilation cage to the top of the ventilation cage before entering the wheat pile. The high-speed airflow area will decrease as the height of the ventilation cage increases. When the height of the ventilation cage is 0.7 m, the area covered by the high-speed flow of the grain pile is larger, and the efficiency of ventilation and cooling is higher.
4. The high-temperature accumulation areas inside the wheat grain pile disappear faster as the ventilation temperature decreases, and the rewetting area near the ventilation cage inside the wheat grain pile gradually expands with the increase in ventilation time.

Author Contributions: Conceptualization, L.L., K.L. and D.Z.; methodology, K.L. and D.Z.; software, K.L., L.L. and D.Z.; validation, K.L. and D.Z.; formal analysis, L.L. and Y.Z.; investigation, K.L. and D.Z.; resources, G.C. and D.Z.; data curation, K.L., L.L. and Y.Z.; writing—original draft preparation, L.L.; writing review and editing, D.Z. and Y.Z.; supervision, G.C. and D.Z.; project administration, D.Z.; funding acquisition, D.Z. All authors have read and agreed to the published version of the manuscript.

Funding: This research was funded by the joint fund project of Henan Science and Technology R&D Program (grant number 222103810082, 222103810073, 232103810078); the Young Backbone Teacher Cultivation Program of Henan University of Technology; the Backbone Training Program of Young Researcher in Henan University of Technology (Grant No. 21420194) and the Henan Key Laboratory of Grain and Oil Storage Facility & Safety (2022KF04).

Institutional Review Board Statement: Not applicable.

Informed Consent Statement: Not applicable.

Data Availability Statement: The data presented in this study are available in the article.

Conflicts of Interest: The authors declare no conflict of interest.

References

1. National Bureau of Statistics of China. *China Statistical Yearbook*; China Statistics Press: Beijing, China, 2022. (In Chinese)
2. Thurner, S.; Laber, M. Indirect effects of the Russia-Ukraine conflict have an impact on global food availability. *Nat. Food* **2023**, *4*, 550–551.
3. Xu, Y.; Wang, Z.X.; Dong, W.J.; Chou, J.M. Predicting the Potential Impact of Emergency on Global Grain Security: A Case of the Russia-Ukraine Conflict. *Foods* **2023**, *4*, 2557. [CrossRef] [PubMed]
4. Liu, W.L.; Chen, G.X.; Liu, C.S.; Zheng, D.Q.; Ge, M.M. Experimental and Numerical Study of Pressure Drop Characteristics of Soybean Grain under Vertical Pressure. *Appl. Sci.* **2022**, *12*, 6830. [CrossRef]
5. Liu, C.S.; Chen, G.X.; Zhou, Y.; Zheng, D.Q.; Zhang, Z.J. Element tests and simulation of effects of vertical pressure on compression and mildew of wheat. *Comput. Electron. Agric.* **2022**, *203*, 107447. [CrossRef]
6. Sharp, J.R. A review of low temperature drying simulation models. *J. Agric. Eng. Res.* **1982**, *27*, 169–190. [CrossRef]
7. Cheng, X.; Zhang, Q.; Shi, C.; Yan, X. Model for the prediction of grain density and pressure distribution in hopper-bottom silos. *Biosyst. Eng.* **2017**, *163*, 159–166. [CrossRef]
8. Giner, S.A.; Denisienia, E. Pressure Drop through Wheat as Affected by Air Velocity, Moisture Content and Fines. *J. Agric. Eng. Res.* **1996**, *63*, 73–85. [CrossRef]
9. Neethirajan, S.; Karunakaran, C.; Jayas, D.S.; White, N.D.G. X-ray Computed Tomography Image Analysis to explain the Airflow Resistance Differences in Grain Bulks. *Biosyst. Eng.* **2006**, *94*, 545–555. [CrossRef]
10. Kashaninejad, M.; Maghsoudlou, Y.; Khomeiri, M.; Tabil, L.G. Resistance to airflow through bulk pistachio nuts (Kalleghochi variety) as affected by moisture content, airflow rate, bed depth and fill method. *Powder Technol.* **2010**, *203*, 359–364. [CrossRef]
11. Ge, M.; Chen, G.; Liu, C.; Zheng, D.; Liu, W. Effect of Vertical Pressure on Temperature Field Distribution of Bulk Paddy Grain Pile. *Appl. Sci.* **2022**, *12*, 10392. [CrossRef]
12. Yue, R.; Zhang, Q. A pore-scale model for predicting resistance to airflow in bulk grain. *Biosyst. Eng.* **2017**, *155*, 142–151. [CrossRef]
13. Montross, M.D.; McNeill, S.G. Permeability of corn, soybeans, and soft red and white winter wheat as affected by bulk density. *Appl. Eng. Agric.* **2005**, *21*, 479–484. [CrossRef]
14. Łukaszuk, J.; Molenda, M.; Horabi, J.; Szot, B.; Montross, M.D. Airflow resistance of wheat bedding as influenced by the filling method. *Res. Agric. Eng.* **2008**, *54*, 50–57. [CrossRef]
15. Khatchatourian, O.A.; Savicki, D.L. Mathematical Modelling of Airflow in an Aerated Soya Bean Store under Non-Uniform Conditions. *Biosyst. Eng.* **2004**, *88*, 201–211. [CrossRef]
16. Lawrence, J.; Maier, D.E. Three-dimensional airflow distribution in a maize silo with peaked, levelled and cored grain mass configurations. *Biosyst. Eng.* **2011**, *110*, 321–329. [CrossRef]
17. Lawrence, J.; Maier, D.E. Prediction of temperature distributions in peaked, leveled and inverted cone grain mass configurations during aeration of corn. *Appl. Eng. Agric.* **2012**, *28*, 685–692. [CrossRef]
18. Ramaj, I.; Schock, S.; Muller, J. Drying Kinetics of Wheat (*Triticum aestivum* L., cv. 'Pionier') during Thin-Layer Drying at Low Temperatures. *Appl. Sci.* **2021**, *11*, 9557. [CrossRef]
19. Ramaj, I.; Schock, S.; Karaj, S.; Muller, J. Influence of Self-Compaction on the Airflow Resistance of Aerated Wheat Bulks (*Triticum aestivum* L., cv. 'Pionier'). *Appl. Sci.* **2022**, *12*, 8909. [CrossRef]
20. Ertekin, C.; Firat, M.Z. A comprehensive review of thin-layer drying models used in agricultural products. *Crit. Rev. Food Sci. Nutr.* **2017**, *57*, 701–717. [CrossRef]
21. Madamba, P.S. Thin layer drying models for osmotically pre-dried young coconut. *Dry. Technol.* **2003**, *21*, 1759–1780. [CrossRef]
22. Rafiee, S.; Keyhani, A.R.; Jafari, A. Modeling effective moisture diffusivity of wheat (Tajan) during air drying. *Int. J. Food Prop.* **2008**, *11*, 223–232. [CrossRef]
23. Chen, C.H.; Wu, P.C. Thin-layer drying model for rough rice with high moisture content. *J. Agric. Eng. Res.* **2001**, *80*, 45–52. [CrossRef]
24. Kumar, D.G.P.; Hebbar, H.U.; Ramesh, M.N. Suitability of thin layer models for infrared-hot air-drying of onion slices. *LWT-Food Sci. Technol.* **2006**, *39*, 700–705. [CrossRef]

25. Dissa, A.O.; Desmorieux, H.; Bathiebo, J. Convective drying characteristics of Amelie mango (*Mangifera indica* L. cv. 'Amelie') with correction for shrinkage. *J. Food Eng.* **2008**, *88*, 429–437. [CrossRef]
26. Erbay, Z.; Icier, F. A review of thin layer drying of foods: Theory, modeling, and experimental results. *Crit. Rev. Food Sci. Nutr.* **2009**, *50*, 441–464. [CrossRef] [PubMed]
27. Bal, L.M.; Kar, A.; Satya, S. Drying kinetics and effective moisture diffusivity of bamboo shoot slices undergoing microwave drying. *Int. J. Food Sci. Technol.* **2010**, *45*, 2321–2328. [CrossRef]
28. Pardeshi, I.L.; Arora, S.; Borker, P.A. Thin-layer drying of green peas and selection of a suitable thin-layer drying model. *Dry. Technol.* **2009**, *27*, 288–295. [CrossRef]
29. Babalis, S.J.; Papanicolaou, E.; Kyriakis, N. Evaluation of thin-layer drying models for describing drying kinetics of figs (*Ficus carica*). *J. Food Eng.* **2006**, *75*, 205–214. [CrossRef]
30. Pabis, S.; Jayas, D.S.; Cenkowski, S. *Grain Drying, Theory and Practice*; John Wiley and Sons Inc.: Hoboken, NJ, USA, 1998.
31. Lukaszuk, J.; Molenda, M.; Horabik, J.; Montross, M.D. Variability of pressure drops in grain generated by kernel shape and bedding method. *J. Stored Prod. Res.* **2009**, *45*, 112–118. [CrossRef]
32. Eisfeld, B.; Schnitzlein, K. A new pseudo-continuous model for the fluid flow in packed beds. *Chem. Eng. Sci.* **2005**, *60*, 4105–4117. [CrossRef]
33. Thorpe, G.R. The application of computational fluid dynamics codes to simulate heat and moisture transfer in stored grains. *J. Stored Prod. Res.* **2008**, *44*, 21–31. [CrossRef]
34. Wang, Y.; Duan, H.; Zhang, H.; Fang, Z. Modeling on Heat and Mass Transfer in Stored Wheat during Forced Cooling Ventilation. *J. Therm. Sci.* **2010**, *19*, 167–172. [CrossRef]
35. Ergun, S. Fluid flow through packed columns. *Chem. Eng. Prog.* **1952**, *48*, 89–94.